Efficient Operation of Lithium-Ion Batteries Based on GPV-Forecasted PV Output

Ahmad Syahiman Mohd Shah[1], Mohamad Shaiful Abdul Karim[1], Mohd Shawal Jadin[1], Airul Sharizli Abdullah[1],
Ruhaizad Ishak[1], Yuki Ishikawa[2], Hiroki Takahashi[2], Suguru Odakura[2] and Naoto Kakimoto[2]
[1]Faculty of Electrical and Electronic Engineering, Universiti Malaysia Pahang, Pekan, Pahang, Malaysia.
[2]Department of Electrical and Electronic Engineering, Ibaraki University, Hitachi, Ibaraki, Japan.
asyahiman@ump.edu.my

Abstract—**Load forecasting is essential in order to fulfil a demand of the consumer. Nevertheless, for a small-scale Battery Energy Storage System (BESS) based on sole photovoltaic (PV), it needs a very strong effort to always meet a consumer's demand due to unstable meteorological conditions. An ideal PV system requires a constructive control strategy in order to alleviate its fluctuating output. In this study, an energy control scheme that executes next-day forecast of generation for the purpose of fully utilizing the stored energy in the batteries has been proposed. Experimental equipment was structured and the operation was completely administered by RX621 microcontroller. The implemented system worked very well without any distractions and it succeeded in controlling and preventing the batteries from being over-charged or over-discharged. Impressively, average consumption for September 2015 is considerably high, which suggests that the proposed control succeeded in utilizing energy corresponded to 98.6 % of the monthly-average generation.**

Index Terms—**Batteries; Energy Management; Photovoltaic; PV Forecasting.**

I. INTRODUCTION

Until now, several studies have been conducted regarding the Home Energy Management System (HEMS) which is commonly focused on control of PV generators, energy consumption visualization or battery storage systems [1-3]. Although the effect of PV generation used does not contribute risky emissions to the environment, it is highly sensitive to the fluctuating atmospheric condition since it partially depends on various meteorological elements such as cloudiness, relative humidity, aerosol, precipitation, atmospheric pressure or air temperature [4-7]. Thus, one of the conventional solutions that can be considered in order to suppress this unsteady output power is to integrate PV panels with parallel-connected rechargeable batteries [8-11]. Instead of focusing on the load side, something needs to be considered on the side of panels/batteries. Since the weather conditions are the main reasons of the fluctuating generated current through the PV panels, it is necessary to predict the weather beforehand in order to prevent an unpredictable electric shortage in the future. In other words, the amount of energy that can be supplied from Energy Storage Units (ESU) to the load should be determined based on a forecasted generation so that the demand of the load will never exceed this limit. Although the use of the relatively small capacity size of ESU may seem to be insufficient in providing the necessary energy to the load, the most important aspect is to keep supplying energy at a certain amount during bad weather conditions by introducing a control algorithm that can cope with this matter. An ideal control algorithm should allow all the generated energy to be fully consumed by the load during sunny sky and also, the same ESU should be able to reserve certain amount energy as a preparation for the incoming unfavourable days that can happen anytime. Consequently, once the proposed control can successfully drive the system to fully utilize the stored energy in the batteries, the next step is to implement it in a scale-up structure.

From our previous work [12], an energy storage system with 20 Ah of capacity was proposed to reduce the Number of Insufficient Days (NID) to a certain amount per year. Nonetheless, the maximum amount of energy that can be captured by this system was relatively small since the effective storage size to store the energy was inadequate as it was limited to 10 Ah. Besides, the daily amount of energy supplied to the load was inflexible since 10 Ah of energy was fixed regardless of any weather conditions. Chronologically, an appropriate storage that is sufficient to accumulate most energy generated during the day or at least the same amount as a yearly-average solar radiation needs to be further considered in order to improve the effectiveness of the entire system. On the other hand, in order to stabilize the daily supplied energy from the PV generator to the load, it is necessary to predict the amount of energy generation for the next day in advance [8]. For example, J. Han et al. has included an estimation of energy generation based on the weather forecast in their HEMS application; but since their systems are not equipped with batteries for energy storage, the focus is mainly on saving the electricity cost by monitoring the home energy use in real-time only [1]. By considering the forecasted generation as a part of the control procedure, any estimation steps that relate to the amount of stored energy in the batteries on the next day can be feasibly arranged beforehand and will be kept on standby mode. Thus, the main objective of this investigation is to implement a control method that executes next-day forecast of generation experimentally so that the flow of energy in the lithium-ion batteries during the charging/discharging process can be strictly monitored, hence, it can be fully utilized by the load for a small-scale BESS.

II. CONTROL ALGORITHM

Conventionally, the actual units of State-Of-Charge, SOC are indicated in percentage points (0 % = empty, 100 % = full). However, in order to make a clear understanding related to the charged/discharged amount of energy in the battery during the generation/consumption process, SOC is

expressed in ampere-hour (Ah) unit in this study and, it is redefined as storage level, E. Two types of SOC estimation method are used in this study; ampere-hour (Ah) counting and Open-Circuit Voltage (OCV). Ah counting method is the most common technique that uses the integral of load current to estimate SOC [13-14]. Nevertheless, since the use of Ah counting method may produce estimation errors which usually starts from the initial stage of the charging/discharging process, the empty, warning and full levels of batteries are determined based on the OCV method. Basically, the storage level, E is expressed as;

$$E = E_0 + G_M - (C_{night} + C_{day})$$
$$E = E_0 + \int_6^{20} I_{in}\, dt - \left(\int_{23}^{t_1} I_{out}\, dt + \int_{12}^{t_2} I_{out}\, dt \right) \quad (1)$$

where E_0, G_M, C_{night}, C_{day}, I_{in} and I_{out} are initial storage level, measured generation, consumption during the night, consumption during the day, input (charging) current and output (discharging) current, respectively. In this study, the charging current is integrated between 6:00 to 20:00 using the basic Ah-counting method as interpreted in the equation above. Meanwhile, the batteries are discharged periodically twice in a day, during the midnight on the previous day (starts from 23:00) and midday (starts from 12:00). Here, since the main focus is emphasized more to the generator and storage components, a loading rheostat with a target current of 5 A is utilized, instead of a variable load for simplification. Therefore, a real-time monitoring of instantaneous energies consumed by multiple electrical appliances that require several complex algorithmic management, for instance, will not be discussed in this paper. The end time for the discharging process on the night, t_1 and day, t_2 are flexible and determined basically by the estimated consumption, C. By assuming that the stored energy in the batteries should be supplied to the load equally during the day and night, the C_{night} and C_{day} in Equation (1) are segregated proportionally from the C where it can be shown as;

$$C_{night} = C_{day} = \frac{C}{2} \quad (2)$$

At this point, the essential step is to decide the most optimized amount of C based on Grid Point Value (GPV)-based calculated generation, G_C so that the remaining energy in the batteries can be fully utilized. The energies of the batteries must be discharged to the load so that all the incoming generated energy of G_C can fill in the batteries. Firstly, the necessary energy to fully charge the batteries, E_N, from initial E, E_0, is defined as;

$$E_N = E_{FULL} - E_0 \quad (3)$$

Next, the target C is determined by the deduction of this E_N from the G_C as;

$$C = G_C - E_N \quad (4)$$

Here, there are several justifications that need to be considered. In order to ensure the load to keep receiving an electric supply every day even during the stormy weather, the minimum consumption C as 10 Ah is underlined, which is one-third from full storage capacity of 30 Ah. Although the amount of this 10-Ah consumption is little, it is sufficient for

the load to use it during an emergency situation. For instance, the energy can be well segregated for a use of a full-charged smartphone for a day (2.8 Ah), CFL bulb 15W for 8 hours (1.2 Ah) and table fan 30W for 20 hours (6 Ah) during summer. On the contrary, the maximum value of C is not restricted to any amount even though the effective storage capacity used here is 30 Ah. For instance, Figure 1 demonstrates the mechanism of proposed control for a five-day period.
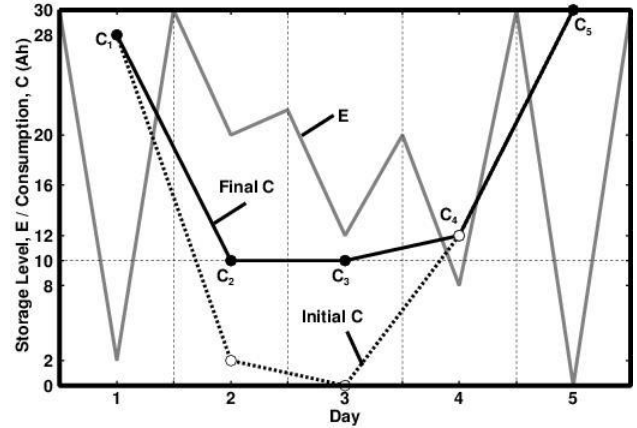

Figure 1: Simple process of determining C based on G_C and E using proposed control. Consumption on the second and third day, C_2 and C_3, are corrected from 2 to 10 and from 0 to 10, respectively. Dotted black line, solid black line and grey line are the initial estimated C, final estimated C and E, respectively.

The G_C for 1st, 2nd, 3rd, 4th and 5th day are exemplified as 28, 2, 8, 22 and 30 Ah, respectively. Without any restriction, C_2 and C_3 are initially estimated as 2 and 0 Ah using Equations (3) and (4) but since the proposed control underlines the minimum C at 10 Ah, the final values of C_2 and C_3 are both corrected to 10 Ah. On the other hand, the case of day 5 in Figure 1 is a simple example for the day with the estimated C with 30 Ah. In order to implement an experiment using this algorithm, the discharge current is manually adjusted using the loading rheostat to become 5 A. 30 Ah of capacity will be expected to completely discharged within 6 hours. Thus, in this case, the end time for t_1 and t_2 in Equation (1) can be approximated as 23:00 + 3 hrs = 2:00 and 12:00 + 3 hrs = 15:00, respectively. In other words, the batteries will be discharged two times, once from 23:00 to 2:00 and another one from 12:00 to 15:00. Eventually, since the G_C for day 5 is estimated as 30 Ah, the storage level of the batteries is expected to be fully recharged again at the end of that day.

III. FORECAST OF PV OUTPUT

A. Solar Radiation Model using Grid Point Value

Numerical weather predictions of solar radiation are performed based on Grid Point Value (GPV) Meso-Scale Model (MSM) developed by Japan Meteorology Agency (JMA). The forecast region is covering entire Japan and the nearest islands from 22.4^O N, 120° E to 47.6^O N, 150° E with the minimum grid size of 5 km. The input location used here is Hitachi, Japan with the coordinates of 36.6^O N, 140.625^O E. The forecasted data includes several meteorological elements such as temperature, cloud cover, relative humidity, air pressure, etc. Nonetheless, since the solar radiation data is not provided from this GPV datasets, the prediction model for this solar radiation needs to be fabricated based on other

meteorological elements. Thus, our recently reported work on solar radiation model [7] will be further applied in this investigation as a part of the experimental procedure. From our previous work [7], the hourly horizontal solar radiation is defined as;

$$S_i = S_c \cos z \cdot f(C) \qquad (5)$$

where S_c and z are the clear-sky solar radiation on earth's surface and solar zenith angle, respectively. By including five parameters, i.e. Relative Humidity (RH), Precipitation (P), low-level cloud cover (CL), middle-level cloud cover (CM) and high-level cloud cover (CH) in this formulation, the function $f(C)$, in Equation (5) can be interpreted as;

$$f(C) = exp\left[-\frac{aRH + bP + cC_L + dC_M + eC_H}{C_0}\right] \qquad (6)$$

where *a, b, c, d* and *e* are variables. One-day horizontal solar radiation is summed up from 6JST to 20JST which can be expressed by Equation (7).

$$S = \sum_{i=6}^{n=20} S_i \left(S_i = \sum_{i=6}^{n=20} S_i \cdot g(l) \right) \qquad (7)$$

for sunny (cloudy/rainy/snowy) days, where the liquid water path, L in gm−2 unit is introduced to the scheme for the case of cloudy, rainy and snowy days as the function $g(l)$ in Equation (8).

$$g(l) = g_0 \cdot exp\left[-\frac{fC_H \cdot L_H + gC_M \cdot L_M + hC_L \cdot L_L}{g_i}\right] \qquad (8)$$

whereby f, g, h are variables and the liquid water path is segregated into three levels; high (L_H), middle (L_M) and low (L_L). Further explanation of this model is elaborated in [7]. Solar radiation, S is then converted to electrical form, which is energy, denoted by generation, G, through the PV panel [12]. Since G and S are directly correlated, a non-linear regression analysis is further considered using local data measured for 328 days at Ibaraki University, Japan from October 1, 2013 to September 30, 2014. As a result, a very good agreement was obtained between the estimated and measured values of G, as shown in Figure 2 with the statistical values of r, R^2, *RMSE* and *MBE* are 0.98, 0.96, 2.30 Ah−1day−1 and 0.11 Ah−1day−1, respectively.
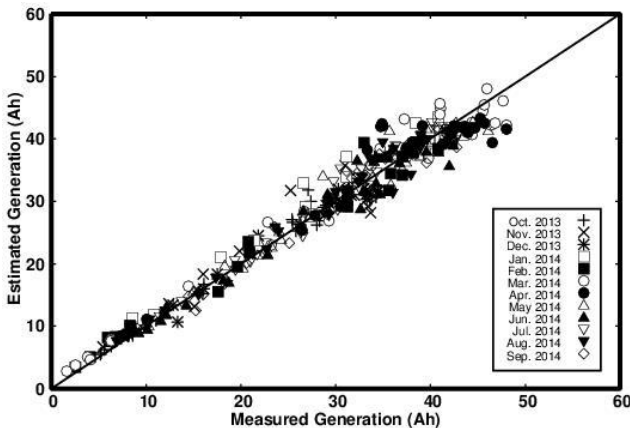

Figure 2: Good correlation was obtained between the estimated and measured values of generation from the data of Oct. 2013 to Sept. 2014.

B. Determination of Weather

Since the solar irradiance model used in this study is divided into two cases, i.e. sunny and rainy/cloudy/snowy days, it is essential to differentiate the weather precisely for a real-time application using the same meteorological elements produced by GPV datasets. Here, the weather is determined using a simple unique technique based on dew-point depression. The dew-point depression is the difference in degrees Celsius (or Kelvin) between the air temperature and dew-point temperature at a certain height in the atmosphere. The dew-point depression for each level can be expressed as;

$$Tdd = T - T_d \qquad (9)$$

where T and T_d are the air temperature and the dew-point temperature, respectively. A cloud base is almost always found in a layer where the dew-point depression, *Tdd* decreases. The *Tdd* usually decreases to between 0° and 6° when a cloud is formed. In other words, a cloud should not be associated with a layer where the *Tdd* decreases since a formation of the cloud occurs only when the decrease leads to a *Tdd* < 6° [15]. On the other hand, several meteorologists in Japan such as S. Daimon, have underlined an assumption that the cloud is completely formed when the *Tdd* drops to 3° or less and precipitation exists if the cloud thickness vertically expands until 2500 m. The hourly values of *Tdd* for the geopotential levels of 300 to 950 MB are mainly taken into account in his work [16]. Subsequently from this idea, in this paper, the rainy/cloudy/snowy day is determined using a number of *Tdd* ≤ 3°, denoted by N_{Tdd}, that occurs at least on two geopotential levels at each effective hour plus 1 extra geopotential level at any effective hour. The hourly-values of dew-point depressions for 300, 400, 500, 600, 700, 800, 900 and 1000 MB geopotential levels are considered in this step. From Equation (9), since one-day solar radiation is summed up from the hourly solar radiation of 6:00, 7:00, 8:00, ..., 20:00 (15 hours' data);

$$N_{Tdd} \geq (15 \times 2) + 1 = 31 \qquad (10)$$

Thus, the determination of sunny or bad weather days is distinguished by the N_{Tdd} value and hence, if the above-mentioned condition in Equation (10) is fulfilled, the one-day solar radiation will be further estimated using Equations (7) and (8).

IV. SIMULATION

Before the experiment is implemented, the proposed control is first compared numerically with a method from our previous study [12]. This method is very simple since the C is set to be 10 Ah every day [8, 12]. The source data of solar radiation is extracted from Hitachi City Hall's weather database [17] and the G_C is estimated basically from Figure 2. Figure 3 represents the number of insufficient days (NID) that occurred over a period of 4 years from 2011 to 2014. The NID is the day when the minimum target of C (10 Ah) cannot be attained [12]. Apparently, the proposed control with measured input data produced NID exactly the same as that of the method [12] with 0 days for all 4 years. The use of measured input data means the G_C is ideal with zero errors. Surprisingly, although the GPV-based forecast data was applied into the control scheme, the NID remained the same
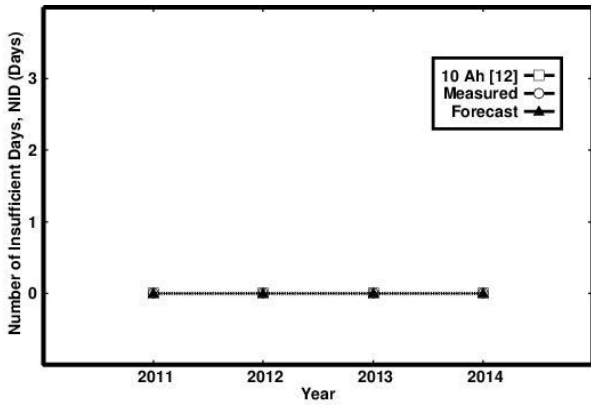
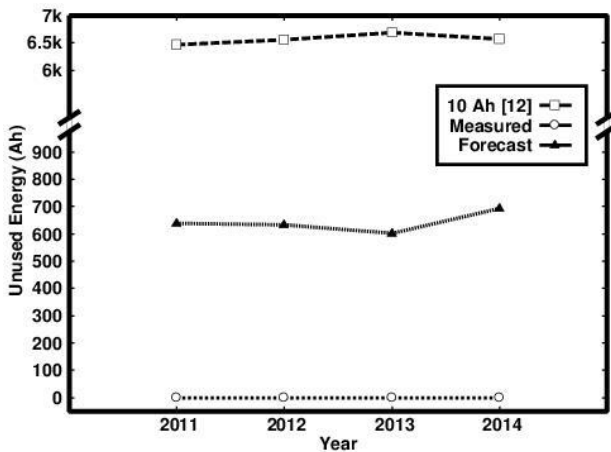Figure 3: The simulation result of number of insufficient days (NID) for 2011-2014.

Figure 4: The simulation result of unused energy for the year of 2011-2014.
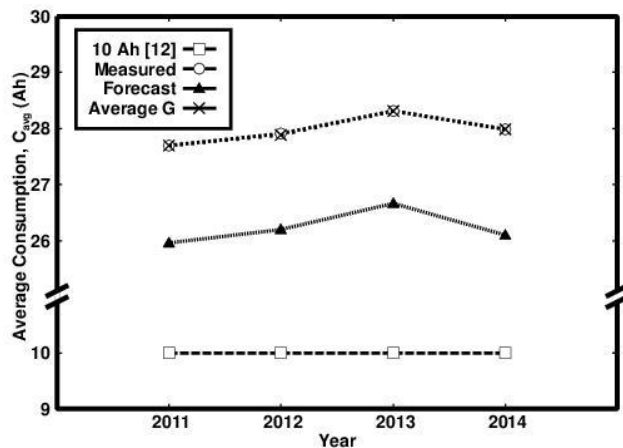

Figure 5: The simulation result of yearly-average energy consumption for the year of 2011 to 2014.

as method [12] and measure lines with 0 day for all years. On the contrary, the forecast differed to the measured curve in term of unused energy with an increment of 1.65 to 1.9 Ah of energy per day, as illustrated in Figure 4. Unused energy is defined as the extra amount of generated energy that cannot be stored by the batteries since the storage level has reached the full state [8]. As can be seen in Figure 4, method [12] wasted lots of energy with approximately 6460 to 6684 Ah (17.85 to 18.31 Ah) of unused energy per year (per day) due to the fixed C (10 Ah). Meanwhile, the measured curve reached the ideal value as no unused energy was ever recorded during these four years. On the other hand, another important element that needs to be considered is a yearly-average consumption, C_{avg}. From Figure 5, it can be suggested that 30 Ah of battery capacity was sufficient to capture most energies through the year in the case of Hitachi as the amount of yearly-average G was in the range of 27.7 Ah to 28.3 Ah. Furthermore, the measured curve succeeded to supply enough energy to the load where the amount of C equals to almost 100% of the average G in all four years. Impressively, when the GPV-forecast data was executed in the scheme, the decline trend was not really significant as it dropped to an acceptable level with a marginal decrease rate of 1.89 Ah at most in 2014 from the measured curve. In other words, it can be said that the proposed method applied with the GPV datasets succeeded to utilize energy that was equivalent to approximately 93.2-94.2% of the average G for 2011-2014. Overall, it can be also suggested that if the precision of G_C can be well improved in the future, the expected values of C_{avg} will nearly approach to the ideal line of 0. Though good results were obtained through numerical analysis, a complete experimented system must be constructed in order to evaluate the effectiveness of the control method and its sensitivity in term of safety when it is integrated with vital equipment like batteries.

V. EXPERIMENTAL SETUP

The experimental equipment of photovoltaic (PV) system structured in this study is represented as Figure 6. This structure basically consists of PV panels, lithium-ion batteries, RX621 microcontroller, MOSFET-based switches, Power Conditioning Unit (PCU) and load. Nevertheless, this is not a full stand-alone type of PV system since external power source from the grid is necessary to power up the small devices such as microcontroller, switches and Xbee 802.15.4 modules. Chronologically, when the batteries are fully charged by the input current from the PV panels, the bypass switch will be turned on soon after the input switch is turned off. Therefore, the input current is bypassed into an electronic DC load, instead of continuously flowing into the batteries and the unused energy will start to be counted until the bypass switch is turned off. Additionally, since it is difficult to connect the microcontroller directly to the internet, the value of G_C that is estimated through the monitoring PC needs to be transmitted to the microcontroller, periodically. Thus, two units of the external wireless data transmitter of Xbee are introduced. The monitoring PC with a Xbee in Figure 6 is placed separately from the main system by several meters in distance. This PC is essential for energy visualization and system's data accumulation.
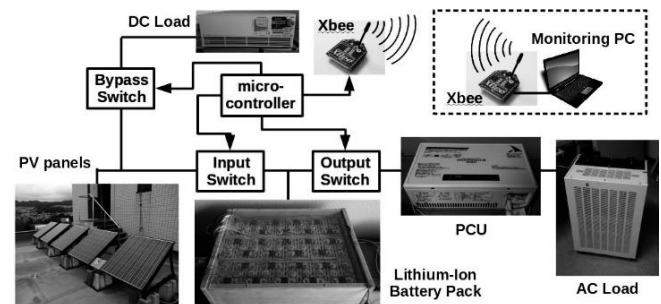

Figure 6: Experimental structure for PV system used in this study.

Five PV panels (SHARP ND-153AU) are series-integrated to the batteries where each panel is rated to supply the maximum values of output power, power voltage and power

current of 153 W, 20.3 V and 7.54 A, respectively. These PV panels are tilted towards the south at approximately 36.6° in order to level the seasonal variation of solar irradiance throughout the year [12]. 30 pieces of lithium-ion batteries (WB-LPY40AHA) with a maximum capacity of 40 Ah are connected in series to form a 100 V DC power supply. The nominal voltage of each battery is standardized at 3.3 V and maximum charge/discharge current can be driven up to 3 CA. Figure 7 represents the discharge test curves for a single battery of WB-LPY40AHA at different current values from 8 A up to 20 A in 4 A intervals. Conventionally, the battery is operated in the range of 4.0 V to 2.8 V but in Figure 7, the battery is discharged from 3.5 V to 3.0 V. From these 4 curves, a non-load condition or known as open-circuit voltage (OCV) curve was derived by eliminating a voltage drop caused by battery's internal resistance during discharging from the method proposed by Tomokazu et al in [18]. By the time the voltage drops to 3.05 V, the OCV line reaches the discharge capacity at approximately 38 Ah. Thus, in order to prevent the battery from over-discharge which may be caused by unpredictable control errors, the capacity of 38 Ah is decided as the new battery's maximum capacity, instead of 40 Ah. Hence, all 30 pieces of batteries will be operated in the range of 3.05 V to 3.4 V. Here, the full battery level (E= 38.0 Ah) is decided when the total battery voltage for these 30 pieces of series-connected batteries reaches 102 V by considering that it is more accurate using the OCV method rather than Ah-counting.
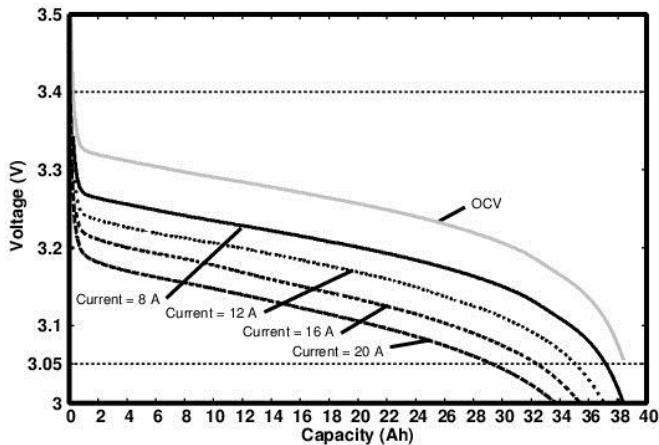

Figure 7: Discharge curves at different current values.

VI. Experimental Setup

To begin, the daily measured and one-day total calculated horizontal solar irradiances for a month (Sept. 2015) is represented in Figure 8. The measured solar irradiance is collected from Hitachi City Hall's database [17] and the calculated solar irradiance is estimated using the calculation model proposed in [7] based on parameterization of relative humidity, precipitation, cloud covers and liquid water path. Since the JMA's web server [20] was inaccessible on Sept. 1, the GPV-MSM datasets failed to be downloaded from this device. Thus, no positive value was estimated in this day and this data will be excluded from the statistical evaluation. The calculated curve exhibited a very good agreement with the measured solar irradiance as relatively high values of the correlation coefficient, r=0.88 and coefficient of determination, $R^2 = 0.74$ was obtained. Furthermore, the calculated values seemed to be slightly overestimated with a

Mean Bias Error, (MBE) of 358.3 Wm⁻²day⁻¹ and a value of Root Mean Square Error (RMSE) was considered low with 900 Wm⁻²day⁻¹. Ordinarily, this calculated horizontal solar irradiance was then converted to the *G* and this *G* value was transmitted to RX621. Figure 9 exhibits the measured and calculated generations derived from the horizontal solar irradiance in Figure 2 for the whole month of September 2015. From this figure, the calculated line is seemed to be overestimated than the measured line with the RMSE and MBE of 2016.7 and 1361.1 Wm⁻²day⁻¹, respectively, but the r value remains the same at 0.88. Surprisingly, almost every day except on 1st, 15th, 21st, 22nd and 26th of Sept., most generated energies through the PV panels were fully utilized by the system whether it was supplied to the load or stored to the battery bank. The unused energy for these days is 4.5, 1.36, 1.91, 0.3 and 1.38 Ah, respectively.
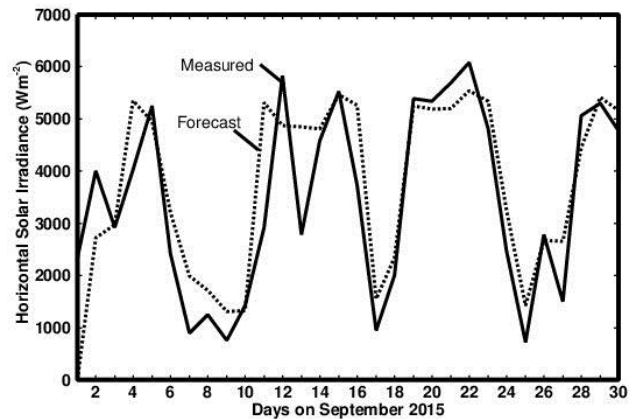

Figure 8: The daily measured and one-day total calculated horizontal solar irradiances for Sept. 1 to 30, 2015 based on [7] forecasting model in Hitachi coordinates.
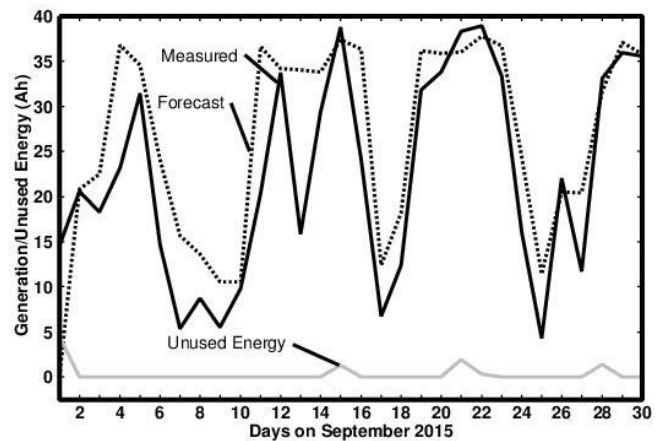

Figure 9: The measured and calculated generations for Sept. 1 to 30, 2015 based on Equation (5).

On the other side, the storage level (SOC or *E*), calculated generation (*FO*), battery voltage (*Vol*), charging current (*I*+), measured generation (*G*), discharging current (*I*-) and consumption (*C*) can be viewed in real-time through an LCD display as shown in Figure 10 or by accessing the logged data in monitoring PC. Apparently, real-time energy visualization is very important for the user to monitor the instantaneous charging/discharging operation of the batteries so that any trouble that might happen during the effective hours can be easily noticed for better prevention. Additionally, Figure 11 presents experimental results of energy control implemented on 1st to 30th in September 2015, respectively. By referring to

the line of storage level, E in this figure, the batteries reached the highest state of storage level on seven days (Sept. 1, 2, 15, 21, 22, 28 and 30). It is obvious that the RX621 microcontroller worked very well with the system as the full level of batteries was successfully controlled to exact values of 38 Ah. Also, no signs of overcharging of the batteries were observed on these days. As mentioned before, since the G_C value for Sept. 1 was not correctly estimated by the monitoring PC before 23:00 on Aug. 31 due to the unavailability of GPV-MSM datasets, the RX621 microcontroller automatically commanded the batteries to be discharged at C=10 Ah where C_{night}=C_{day}=5 Ah. Moreover, Hitachi experienced very good weather conditions during this month as the E line did not drop lower than 10 Ah in all days except Sept. 11 and no NID was ever counted here. The highest C was recorded on Sept. 22 with 37.2 Ah. On the contrary, there were 9 days in this month that performed 10 Ah of C which was commonly caused by the unfavourable weather conditions. This value is the minimum must-used amount of C that is explicitly underlined through this control scheme in order to ensure that the energy still can be supplied to the load although the weather is unstable. On the other hand, the C_{avg} for Sept. 2015 is considerably high with approximately 21.9 Ah, which suggests that the proposed control succeeded in utilizing energy corresponded to 98.6% of the average G of 22.2 Ah.

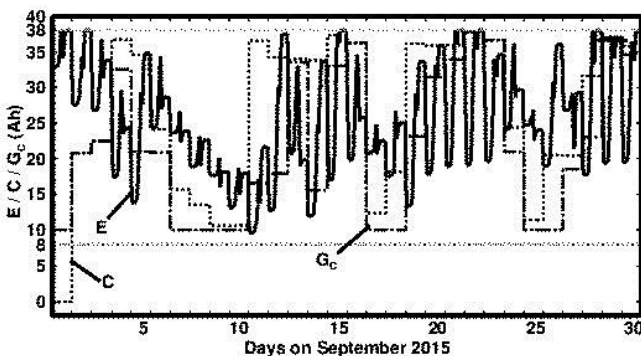Figure 10: LCD display that visualizes several system and energy information.

Figure 11: Result of energy control on September 1-30, 2015. Solid, dashed and dash-dotted lines are the storage level, E, calculated generation, G_C and consumption, C, respectively. No signs of overcharging of the batteries were observed on Sept. 1, 2, 15, 21, 22, 28 and 30 as the storage level did not exceed its highest state of 38 Ah.

VII. CONCLUSION

In this paper, an energy control that considers the next-day forecast of generation for the purpose of fully utilizing the stored energy in batteries has been proposed. The main target is to implement this forecast data experimentally so that the flow of energy in the lithium-ion batteries during the charging/discharging process can be strictly monitored,

hence, the energy can be fully utilized by the load. The experimental results show a very good agreement with the simulated results (r=0.88). Furthermore, the implemented system worked very well without any problem and it succeeded in controlling and preventing the batteries from being over-charge or over-discharge. Thus, it is desirable if the entire proposed system might become a trigger for other researchers to structure more comprehensive Energy Management System (EMS) applications that are more reliable, efficient and sophisticated in the future.

REFERENCES

[1] J. Han, C-S. Choi, I. Lee and S-H. Kim, "Smart Home Energy Management System Including Renewable Energy Based on ZigBee and PLC," *IEEE Trans. Consum. Electron.*, vol. 60, no. 2, pp. 198-202, May 2014.
[2] J. Han, C-S. Choi and I. Lee, "More Efficient Home Energy Management System Based on Zigbee Communication and Infrared Remote Controls," *IEEE Trans. Consum. Electron.*, vol. 57, no. 1, pp. 85-89, Feb. 2011.
[3] H. Kim, S. K. Lee, H. Kim and H. Kim, "Implementing home energy management system with UPnP and mobile applications," *ScienceDirect Comput Commun.*, vol. 36, pp. 51-62, 2012.
[4] H-L. Jou, Y-H. Chang, J-C. Wu and K-D. Wu, "Operation strategy for a lab-scale grid-connected photovoltaic generation system integrated with battery energy storage," *ScienceDirect Energy Convers. Manag.*, vol. 111, pp. 853-861, 2013.
[5] H. Ohtake, K. Shimose, J. G. d. S. Fonseca Jr., T. Takashima, T. Oozeki and Y. Yamada, "Accuracy of the solar irradiance forecasts of the Japan Meteorological Agency mesoscale model for the Kanto region, Japan," *ScienceDirect Solar Energy*, vol. 98, pp. 138-152, Dec. 2013.
[6] J. Almorox, "Estimating global solar irradiation from common meteorological data in Aranjuez, Spain," *Turkish J. Phys.*, vol. 35, pp. 53-64, 2011.
[7] A. S. B. M. Shah, H. Yokoyama and N. Kakimoto, "High-Precision Forecasting Model of Solar Irradiance Based on Grid Point Value Data Analysis for an Efficient Photovoltaic System," *IEEE Trans. Sustain. Energy*, vol. 6, no. 2, pp. 474-481, Apr. 2015.
[8] A. S. M. Shah, Y. Ishikawa, S. Odakura and N. Kakimoto, "Numerical Model of Energy Control for Lithium-Ion Batteries Based on PV System," *Int. J. SIM. Syst. Sci. Technol.*, to be published.
[9] Q. Guo, S. Chen and X. Qin, "ZnOSnO2/graphene composites as high capacity anode materials for lithium-ion batteries," *ScienceDirect Mater. Lett.*, vol. 128, pp. 50-53, 2014.
[10] K. Darcovich, E. R. Henquin, B. Kenney, I. J. Davidson, N. Saldanha and I. B-Morrison, "Higher-capacity lithium-ion battery chemistries for improved residential energy storage with micro-cogeneration," *ScienceDirect Appl. Energy*, vol. 111, pp. 853-861, 2013.
[11] X. Li, D. Hui and X. Lai, "Battery Energy Storage Station (BESS)-Based Smoothing Control of Photovoltaic (PV) and Wind Power Generation Fluctuations," *IEEE Trans. Sustain. Energy*, vol. 4, no. 2, pp. 464-473, Apr. 2013.
[12] N. Kakimoto, S. Matsumura, K. Kobayashi and M. Shoji, "Two-state Markov Model of Solar Radiation and Consideration on Storage Size," *IEEE Trans. Sustain. Energy*, vol. 5, no. 1, pp. 171-181, Jan. 2014.
[13] S. Piller, M. Perrin and A. Jossen, "Methods for state-of-charge determination and their applications," *J. Power Sources*, vol. 96, pp. 113-120, 2001.
[14] H. Wang, Y. Liu, H. Fu and G. Li, "Estimation of State of Charge of Batteries for Electric Vehicles," *Int. J. Control Autom.*, vol. 6, no.2, pp. 185-194, Apr. 2013.
[15] J. W. Overall, "The Used of The skew T, Log P Diagram in Analysis and Forecasting," HQ AWS/XT, Scott AFB, IL, Tech. Rep., AWS/TR-79/006, Mar. 1990.

[16] S. Daimon, "Time-Sequence Forecast based on Cloud's Sectional View: Utilization of Numerical Prediction (in Japanese)," *Tenki*, vol. 54, pp. 975-976, Nov. 2007.

[17] Hitachi City Hall. (2015, Mar.) *Index of Observed Weather Database for Hitachi* (Japanese) [Online]. Available: http://www.jsdi.or.jp/~hctenso/.

[18] M. Tomokazu, M. Yukitaka and H. Keizoh, "Estimation of State of Charge of Batteries for Electric Vehicles (in Japanese)," *Toshiba Rev.*, vol. 68, no. 10, pp. 54-57, 2013.

[19] Renesas Elect. Corp. (2010, Feb.). *RX62N, RX621*. [Online]. Available: http://am.renesas.com/products/mpumcu/rx/rx600/rx62162n/index.jsp

[20] Japan Meteorology Agency (JMA). (2015, Feb.) *Index of Weather Data based on GPV Numerical Prediction* [Online]. Available: http://database.rish.kyoto-u.ac.jp/arch/jmadata/data/gpv/original/.